

Robust Continuous Motion Strategy Against Muscle Rupture using Online Learning of Redundant Intersensory Networks for Musculoskeletal Humanoids

Kento Kawaharazuka^{a,*}, Manabu Nishiura^a, Yasunori Toshimitsu^a, Yusuke Omura^a,
Yuya Koga^a, Yuki Asano^a, Kei Okada^a, Koji Kawasaki^b, Masayuki Inaba^a

^aDepartment of Mechano-Informatics, Graduate School of Information Science and Technology, The University of Tokyo, Japan
^bTOYOTA Motor Corporation, Aichi 471-8751, Japan

Abstract

Musculoskeletal humanoids have various biomimetic advantages, of which redundant muscle arrangement is one of the most important features. This feature enables variable stiffness control and allows the robot to keep moving its joints even if one of the redundant muscles breaks, but this has been rarely explored. In this study, we construct a neural network that represents the relationship among sensors in the flexible and difficult-to-modelize body of the musculoskeletal humanoid, and by learning this neural network, accurate motions can be achieved. In order to take advantage of the redundancy of muscles, we discuss the use of this network for muscle rupture detection, online update of the intersensory relationship considering the muscle rupture, and body control and state estimation using the muscle rupture information. This study explains a method of constructing a musculoskeletal humanoid that continues to move and perform tasks robustly even when one muscle breaks.

Keywords: Musculoskeletal Humanoid, Redundancy, Neural Networks

1. Introduction

The musculoskeletal humanoid [1, 2, 3, 4, 5] has various biomimetic advantages such as variable stiffness using redundant muscles, ball joints without singular points, underactuated and flexible fingers, etc. In this study, we develop a robust learning control strategy focusing on the muscle redundancy, which is one of the characteristics of musculoskeletal humanoids. In a musculoskeletal structure where the control input (muscle length) is redundant with respect to the joint angle to be controlled, even if one muscle is broken, it can be compensated and the robot can continue to move as before, leading to a more robust robot configuration (Fig. 1). In order to make use of this characteristic for musculoskeletal humanoids, which are flexible and difficult to modelize, we propose a new learning-based framework. In this study, online learning of a musculoskeletal intersensory network, as well as muscle length-based control, state estimation, and anomaly detection using it are described, forming a strategy against muscle rupture. The muscle redundancy is utilized to realize continuous motions in an actual musculoskeletal humanoid, Musashi [1]. From the experiments, we show that the algorithm of online learning, state estimation, and control can be modified based on the information of muscle rupture to adapt to the current body state, without destroying the network structure. This enables a series of continuous movements even if one muscle is broken.

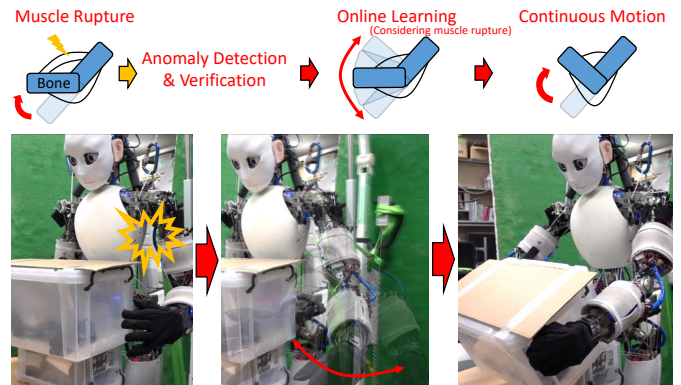


Figure 1: The overall concept of this study: anomaly detection for muscle rupture, verification of the muscle rupture state, online learning of intersensory networks considering muscle rupture, and robust continuous motion control using them.

1.1. Redundancy of Musculoskeletal Structures

The muscle redundancy has been mainly focused on variable stiffness control [6] and biarticular muscles [7] so far. Also, since the muscle redundancy is difficult to handle for control in some cases, many methods have been proposed to eliminate it [8, 9]. On the other hand, another important feature of the muscle redundancy is that the robot can continue to move even if one of the muscles is broken, but this has been rarely explored. [10] refers to a possibility to include information of muscle rupture in muscle tension-based control, but there is no evaluation of this feature, no discussion on judging whether the muscle is broken or not (anomaly detection and its verification), and no relearning of the body model after the muscle rupture.

*Corresponding author.

Email address: kawaharazuka@jsk.imi.i.u-tokyo.ac.jp
(Kento Kawaharazuka)

1.2. Control, State Estimation, and Anomaly Detection for Flexible Musculoskeletal Structures

Various studies have been conducted to control the flexible musculoskeletal structure which is difficult to modelize. There are some studies [11, 12, 10] of muscle tension-based control methods. These studies make use of joint-muscle mappings [13] learned in actual robots as muscle Jacobian. However, it is difficult to control such robots as intended due to the large friction and hysteresis between the muscles and various parts of the body [10]. Therefore, this study is based on muscle length-based control.

As a method of muscle length-based control, Motegi et al. proposed a method to realize an accurate hand position by updating a table that correlates the position with muscle length [14]. Mizuuchi et al. represented the relationship between joints and muscles with neural networks from motion capture data and performed accurate body control [15]. Kawaharazuka et al. have developed a method to control the body by learning a neural network that represents the relationship between joints and muscles online [16], and extended it to take into account the change in muscle route due to the flexibility of the body tissue [6, 17]. This online learning mechanism is essential for musculoskeletal humanoids, where the relationship among body sensors are constantly changing. However, [14] is unsuitable to consider muscle rupture because it directly rewrites the data table of the hand position and muscle length, and thus all data must be rewritten when one muscle is broken. [15, 16] cannot handle muscle tension. [6, 17] can handle muscle tension but cannot handle the change in the control command when one muscle is broken, because the muscle length command is obtained by only forwarding a neural network once.

Other methods have been developed to dynamically control simple pneumatic robots with one or two degrees of freedom using Gaussian Process Regression (GP) [18], neural networks and sequential quadratic programming [19], etc., but they have only been experimented with low degrees of freedom (even with a robot with many degrees of freedom, different controllers have been created for each joint). Also, they have not been able to deal with the physical changes (e.g. muscle rupture) and online learning of the body model (it is especially difficult to deal with online learning and physical changes flexibly in GP). If we want to obtain a dynamic model of a complex body such as a musculoskeletal humanoid, we need a large amount of data, and the model is usually overfitted by online learning due to the model complexity. For redundant systems other than the musculoskeletal robot, there are options such as dynamic neural networks (DNN) [20], dynamic movement primitives (DMP) [21], and reinforcement learning (RL). However, DNN makes a number of assumptions on the body model, DMP is not suitable to relearn the body model online after a change in the body, and RL takes an unrealistically long time to learn for complex actual systems. From these perspectives, this study uses muscle length-based control instead of a muscle tension-based one, a static model instead of a dynamic one, and a neural network instead of other modeling methods.

Musculoskeletal AutoEncoder (MAE) [22] is used as a core method of this study, which extends [6, 17]. This allows for

a unified method for state estimation, control, and simulation of musculoskeletal humanoids using the mutual relationship among joint angle, muscle tension, and muscle length. We utilize the feature that the state estimation and control are performed by optimization based on the minimization of loss function, and we modify the algorithm in order to handle muscle rupture by changing the definition of the loss function. For anomaly detection, some methods such as [23, 24, 25] have been proposed, but the classical method [23] requires an accurate dynamic model of the body, and learning models [24, 25] have been developed as different models from state estimation and control. Our method is effective in that it eliminates the need for individual model management, since state estimation, control, and anomaly detection are performed in a single unified network. In this study, the functions of MAE have been extended by improving the framework of state estimation, control, and anomaly detection, and by adding the change in all components to make use of the muscle redundancy. We call our proposed network Redundant Musculoskeletal AutoEncoder (RMAE).

1.3. Our Contribution

This study discusses a new robust motion strategy that explicitly exploits the redundancy of the muscle, which has not been handled much so far. The system detects the anomaly, verifies the muscle rupture state, relearns the body model after the muscle rupture, and then resumes the behavior as before. A comprehensive discussion is also given on the hardware, software, and network architecture for the robust motion strategy. The contributions of this study are as follows.

- Modularized hardware and learning software system design to take advantage of the muscle redundancy
- Online learning of the musculoskeletal intersensory network using the mutual relationship among joint angle, muscle tension, and muscle length, as well as control, state estimation, and anomaly detection using the same model
- Changes in online learning, control, and state estimation after muscle rupture using muscle rupture verification and changes in loss function with the muscle rupture information
- Robust motion experiments using the muscle redundancy of the actual musculoskeletal humanoid

2. Basic Musculoskeletal Structure

In the musculoskeletal structure, redundant muscles are antagonistically arranged around the joints (Fig. 2). Not only monoarticular muscles across one joint but also polyarticular muscles across multiple joints exist. For the number of degrees of freedom (DOFs) of joints D , the minimum number of muscles required to move them is $D + 1$, but most musculoskeletal humanoids have more muscles than that. In other words,

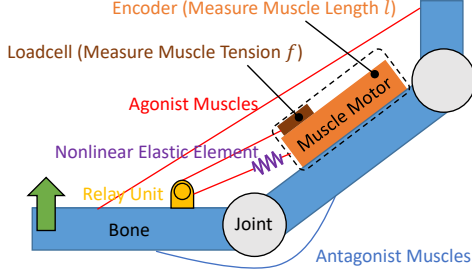


Figure 2: The basic musculoskeletal structure.

even if one of the muscles is broken, the robot can still move with the other muscles, whereas for axis-driven robots, when one joint is broken, they must stop the movement. The muscles are mainly composed of Dyneema, which is an abrasion resistant synthetic fiber. Nonlinear elastic elements that allow variable stiffness control are often arranged in series with the muscles. In some robots, the muscles are folded back with muscle relay units composed of pulleys in order to gain momentum arm. The muscles are sometimes wrapped with soft foam covers for the flexible contact, which make the robot more difficult to modelize. For each muscle, an encoder can measure muscle length l , a loadcell can measure muscle tension f , and a thermal sensor can measure muscle temperature c . Although joint angles θ cannot be measured in many cases due to the ball joint and complex scapula, some robots can measure them using special mechanisms [1, 26]. Also, by using a vision sensor, it is possible to estimate the joint angle, which can be used as the actual joint angle. In this method, AR markers, which can get its six-dimensional position from vision, are attached to the end-effector of the robot. The marker position \mathbf{P}_{marker} is obtained from vision, and the inverse kinematics is solved for $\mathbf{P}^{ref} = \mathbf{P}_{marker}$ by using the estimated joint angle θ^{est} from the change in muscle length [13] as the initial value θ^{init} , as shown below,

$$\theta^{est'} = \text{IK}(\mathbf{P}^{ref} = \mathbf{P}_{marker}, \theta^{init} = \theta^{est}) \quad (1)$$

where IK expresses inverse kinematics and $\theta^{est'}$ is the estimated joint angle corrected by vision. Note that this study updates the relationship between joints and muscles, but assumes that the geometric model for joint position and link length is correct.

3. Utilization of Muscle Redundancy in Musculoskeletal Humanoids

The overall flow of this study is shown in Fig. 3. The musculoskeletal humanoid with the flexible body is considered to have the following requirements for a robust motion strategy that allows it to continue to move even when one muscle is ruptured.

- The ability to detect muscle rupture.
- The ability to relearn the body model after the muscle rupture.

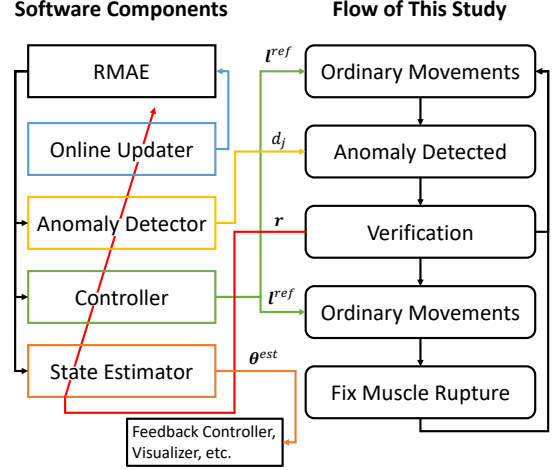


Figure 3: Overview of software components and flow of this study. The muscle rupture information r from Verification (red line) changes each component of online updater, anomaly detector, controller, and state estimator.

- Ease of muscle replacement.

First, it is necessary to be able to detect muscle rupture, but there can be various states of muscle rupture in musculoskeletal robots. In this study, muscle rupture is comprehensively defined as the state in which the muscle is broken due to friction or external force and the state in which the muscle cannot be moved due to malfunction of the circuit or motor, etc. Once the muscle rupture is detected, the motion is stopped, the state of the muscle is checked, and then the next motion strategy can be planned. Next, the relationship among muscle length, muscle tension, and joint angle in the flexible body should be relearned after the muscle rupture, because the relationship among them has been changed. Then, the body should be able to move as before the muscle rupture. Finally, if more than one muscle have been ruptured, the body will not be able to continue moving. Therefore, the muscles must be easily replaceable by humans.

There are several other strategies that can be considered. The first strategy is to stop the robot until the muscles are replaced, without relearning the body model. This is a conventional approach, and while the algorithm is very simple, it does not use the robot to its full potential. The second strategy is to keep learning the body model without detecting the muscle rupture. This simplifies the algorithm as in the first strategy, but our experiments in Sec. 4 show that if the body model continues to be learned without including the muscle rupture information, the model changes significantly and the control and state estimation cannot be performed as intended. The third strategy is to self-heal muscles like humans without replacing muscles [27]. If this approach could be applied to this study, a complete system without human intervention could be constructed. However, the current technology has several problems, such as large unit size and large decrease in the transmissible tension after self-healing compared to before the muscle rupture. Therefore, in this study, we describe a strategy for robust continuous motion using muscle redundancy, based on the approach of muscle rupture detection, online learning of the body model

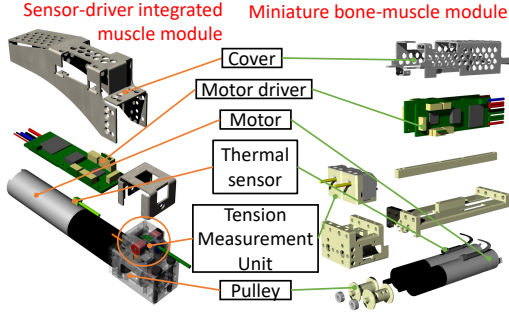


Figure 4: A sensor-driver integrated muscle module [28] and a miniature bone-muscle module [29] for ease of replacement.

including muscle rupture information, and subsequent muscle replacement.

3.1. Hardware and Software Requirements

Regarding hardware, for the ease of muscle replacement, sensor-driver integrated muscle module [28] and miniature bone-muscle module [29] have been developed (Fig. 4). They are muscle modules which include motors, motor drivers, temperature sensors, and muscle tension measurement units in one package to improve reliability and maintainability. The previous muscle actuator [30] has not been modularized and the motors and motor drivers have been located in different places, which requires a lot of effort to replace them. In contrast, for [28, 29], all that is required is to remove four screws, and replace and install the module again. From preliminary experiments, an experienced researcher was able to replace the whole module in about four minutes. In this study, the musculoskeletal humanoid Musashi [1], which is equipped with these muscle modules, is used in the experiments.

Regarding software, the main components required for this study are control, state estimation, and anomaly detection of the flexible body (state estimation is not directly necessary in this study, but is important in most cases for visualizer, feedback control, etc.). They are also updated online via a variable network structure such as a neural network and must be always adapted to the current body state. The muscle rupture cannot be completely determined only by detecting anomaly, so it is also important to verify the muscle rupture state afterwards. Finally, since some of the sensor values are improbable after the muscle rupture, all components such as online learning, anomaly detection, control, and state estimation should be modified accordingly.

3.2. Redundant Musculoskeletal Autoencoder

The structure of RMAE (Redundant Musculoskeletal AutoEncoder), which is the core of this work, is shown in Fig. 5. The structure itself is equivalent to MAE of [22], but the main technical novelty of this study is the addition of anomaly detection and muscle rupture verification using RMAE, and the changes based on muscle rupture information in online learning, control, and state estimation. The notations in this article are shown in Table 1.

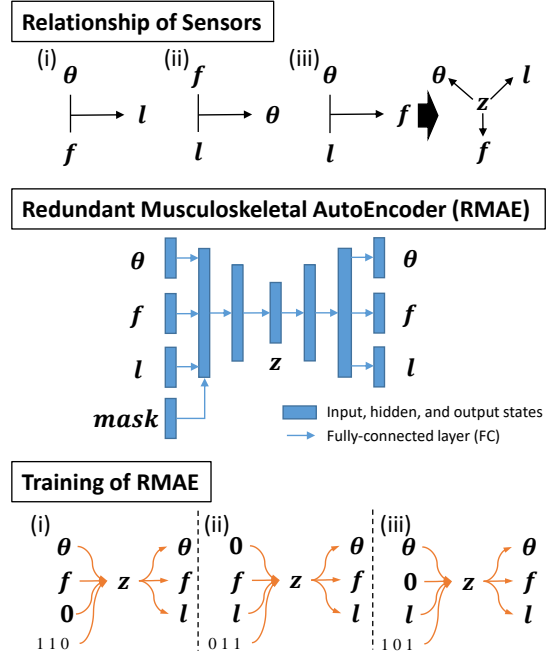


Figure 5: The relationship of sensors, the network structure of RMAE, and the training of RMAE.

RMAE represents an intersensory relationship among redundant sensors, and we focus on the joint angle θ , muscle tension f , and muscle length l that are usually obtained in musculoskeletal humanoids as shown in Sec. 2. There exist three relationships of (i) $(\theta, f) \rightarrow l$, (ii) $(f, l) \rightarrow \theta$, and (iii) $(l, \theta) \rightarrow f$, as shown in the upper diagram of Fig. 5. That is, among the three sensor values (θ, f, l) , one can be inferred from the other two, which corresponds to the fact that all three sensor information can be obtained from two of the three sensors. The latent variable z can be calculated from two of the three sensors and z has information of all three sensors.

Thus, condensing these three relationships into a single network, an AutoEncoder-type network [31] that inputs (θ, f, l) and $mask$ and outputs the same (θ, f, l) , as shown in the middle diagram of Fig. 5, is constructed. $mask$ is a variable that switches between (i) – (iii) in Fig. 5. Let D be the number of joints and M be the number of muscles, and the number of dimensions of $(\theta, f, l, mask)$ are $(D, M, M, 3)$. Let z be the value of the middle layer with the smallest number of units in RMAE, with a dimension of $D + M$. This is because the minimum number of units can be smaller than $D + M$ since all values of (θ, f, l) can be inferred from (θ, f) . In this study, RMAE consists of seven fully-connected (FC) layers including the input and output layers, and the number of units is set to $(D + 2M + 3, 200, 30, D + M, 30, 200, D + 2M)$. The numbers of units in the middle layers such as 30 and 200 are experimentally determined to be the minimum value that can explain the obtained data reasonably well. As the number of units increases, the accuracy improves, but the amount of computation increases, and over-fitting tends to occur. The activation function other than the last layer is hyperbolic tangent. The unit of θ is [rad], the unit of f is [N/200], and the unit of l is [mm/100],

Table 1: Notations in this article.

Notation	Definition
D	the number of joints
M	the number of muscles
θ	joint angle $\in \mathcal{R}^D$
θ^{est}	the estimated joint angle $\in \mathcal{R}^D$
l	muscle length $\in \mathcal{R}^M$
f	muscle tension $\in \mathcal{R}^M$
c	muscle temperature $\in \mathcal{R}^M$
$mask$	the mask vector inputted in RMAE $\in \{0, 1\}^3$
z	the latent value of RMAE $\in \mathcal{R}^{D+M}$
r	the muscle rupture state $\in \{0, 1\}^M$
τ^{ref}	target joint torque $\in \mathcal{R}^D$
G	muscle Jacobian $\in \mathcal{R}^{M \times D}$
$h_{\{enc, dec\}}$	the encoder or decoder part of RMAE
$\{\theta, f, l\}^{data}$	data of $\{\theta, f, l\}$ accumulated for training of RMAE
$\{\theta, f, l\}^{cur}$	the current measured sensor data of $\{\theta, f, l\}$
$\{\theta, f, l\}^{pred}$	$\{\theta, f, l\}$ predicted from RMAE
$\{\theta, f, l\}^{ref}$	target value of $\{\theta, f, l\}$
$\{\theta, f, l\}_i$	the i -th value of $\{\theta, f, l\}$

in order to roughly adjust the scale. The current network structure of RMAE takes about 1.5 msec for a single inference and 3.0 msec for a single backpropagation, with the deep learning framework Chainer [32]. The algorithm itself consumes very little memory, while the network takes up about 10–100 Kbytes of memory depending on the number of input and output dimensions.

Next, we describe the outline of the training method of RMAE. Although the structure of RMAE is similar to that of the usual AutoEncoder, the training method is special because of the presence of *mask*. Using the fact that all three sensor information can be obtained from two of (θ, f, l) , as shown in (i) in the lower diagram of Fig. 5, when the sensor information is narrowed down to (θ, f) , $(\theta, f, \mathbf{0})$, $(1 \ 1 \ 0)^T$ is taken as input and (θ, f, l) is output. The value set to 0 in *mask* needs to be $\mathbf{0}$. (ii) and (iii) are run in the same way while changing the *mask*, and the training is performed so that the input and output are close to each other. First, RMAE is initially trained from a geometric model including the relationship between joints and muscles. After that, the actual sensor data is obtained and this network is updated online.

Some functions used in this study are defined as follows,

$$z = h_{enc}(\theta, f, l, mask) \quad (2)$$

$$z = h_{enc,i}(\theta, f) = h_{enc}(\theta, f, \mathbf{0}, (1 \ 1 \ 0)^T) \quad (3)$$

$$z = h_{enc,ii}(f, l) = h_{enc}(\mathbf{0}, f, l, (0 \ 1 \ 1)^T) \quad (4)$$

$$z = h_{enc,iii}(\theta, l) = h_{enc}(\theta, \mathbf{0}, l, (1 \ 0 \ 1)^T) \quad (5)$$

$$(\theta, f, l) = h_{dec}(z) \quad (6)$$

$$\theta = h_{dec,\theta}(z) \quad (7)$$

$$f = h_{dec,f}(z) \quad (8)$$

$$l = h_{dec,l}(z) \quad (9)$$

where h_{enc} is the encoder part of RMAE, and $h_{enc,\{i, ii, iii\}}$ expresses each condition of encoder corresponding to (i), (ii), or (iii) in Fig. 5. Also, h_{dec} is the decoder part of RMAE, and

$h_{dec,\{\theta, f, l\}}$ expresses each decoder outputting $\{\theta, f, l\}$.

A detailed overall software system surrounding RMAE is shown in Fig. 6. RMAE is at the center of this system and each of its components is executed by using backpropagation technique [33].

3.3. Initial Training of RMAE

In order to update RMAE online, it is necessary to initialize RMAE with a geometric model of the musculoskeletal structure. The geometric model represents each muscle route by linearly connecting the start, relay, and end points of the muscle. The relationship between muscle length change and muscle tension in a nonlinear elastic element is identified and combined with the geometric model to obtain the data on (θ, f, l) while randomizing θ and f in the geometric model.

Using these data, (i), (ii), and (iii) in Fig. 5 are randomly executed. In other words, one of (θ, f, l) is randomly set to $\mathbf{0}$, the data including the corresponding *mask* is inputted to RMAE, and the predicted data $(\theta^{pred}, f^{pred}, l^{pred})$ is outputted. Finally, RMAE is trained by calculating the loss function $L_{initial}$ for $\{\theta, f, l\}$ as follows,

$$L_{initial} = w_{\theta} \|\theta - \theta^{pred}\|_2 + w_f \|\mathbf{f} - \mathbf{f}^{pred}\|_2 + w_l \|l - l^{pred}\|_2 \quad (10)$$

where $\|\cdot\|_2$ represents L2 norm.

In this study, the number of batches for initial training is set to $N_{batch}^{init} = 100$, the number of epochs is set to $N_{epoch}^{init} = 100$, $w_{\theta} = 1.0$, $w_f = 10.0$, $w_l = 100.0$, and the optimization method is Adam [34]. Various values were tried for these parameters, and they are adjusted to make each error for $\{\theta, f, l\}$ less than about 0.01. The model of the epoch with the smallest test loss was used. For the activation function and the optimization method, we tried various types and selected the algorithm that converges to the smallest loss.

3.4. Online Learning of RMAE

We describe the online learning of RMAE using the sensor information of the actual robot.

First, the current sensor data $(\theta^{cur}, f^{cur}, l^{cur})$ is obtained from the actual robot. Note that the training data is generated when the robot is stationary and the joint angle or the muscle tension is farther than a certain threshold from the previous training data.

Next, this data is accumulated and augmented, and RMAE is updated online. The data $(\theta^{cur}, f^{cur}, l^{cur})$ is accumulated and when the number of data exceeds N_{thre}^{online} , the online update is started. N_{data}^{online} ($N_{data}^{online} \leq N_{thre}^{online}$) random data from the accumulated data and the latest data are obtained. Also, one data point of $(\mathbf{0}, \mathbf{0}, \mathbf{0})$ is added. To these data, three *mask* of (i), (ii), and (iii) are added, respectively, and a total of $3 \times (N_{data}^{online} + 2)$ data is used to update the network in the same way with Sec. 3.3, with the loss function L_{online} as $L_{initial}$. Since the initial training builds up the overall network structure, the network smoothly matches the obtained data by online learning without destroying the structure.

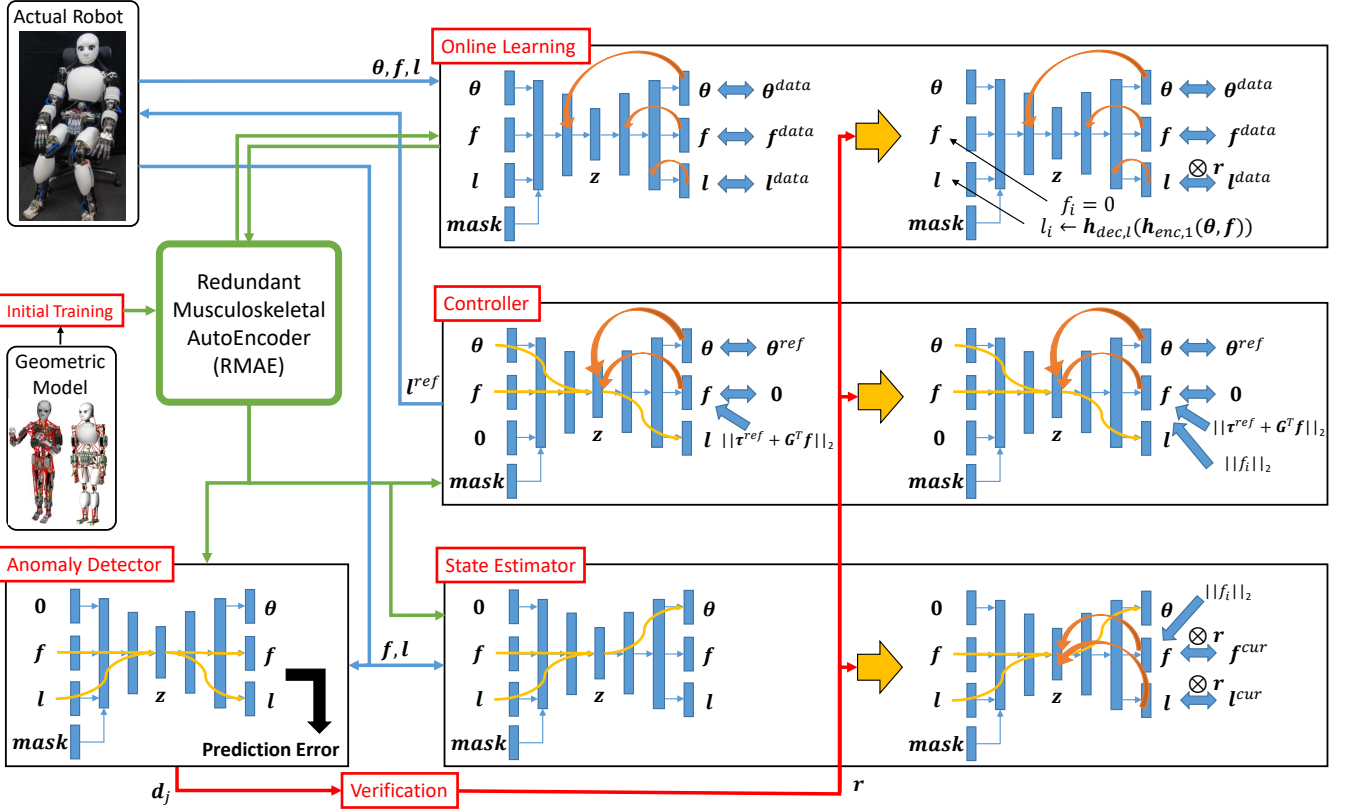


Figure 6: The detailed overall software system.

Here, it is necessary to change the online learning method depending on the muscle rupture information \mathbf{r} (an M -dimensional vector with 0 for ruptured muscles and 1 for unruptured muscles). The changes in online learning, state estimation, and control based on \mathbf{r} are the most important technical novelties of this study that take advantage of the muscle redundancy. When a muscle is ruptured, f is always close to zero and l does not change at all, so if the online learning continues as it is, the structure of RMAE will be severely destroyed. So first, for the obtained dataset $(\theta, \mathbf{f}, \mathbf{l})$, let \mathbf{f} of the ruptured muscle i , f_i , be 0. Next, since l of the ruptured muscle i , l_i , cannot be directly used, l_i^{pred} is inferred as $l_i^{pred} = h_{dec,l}(h_{enc,i}(\theta, \mathbf{f}))$. Finally, l_i is replaced with l_i^{pred} (l_i^{pred} of the muscle i), and online learning is executed. Here, the loss related to l of muscle i is not meaningful and must be removed from the loss function. Therefore, the loss function is written as follows,

$$L'_{online} = w_\theta \|\theta - \theta^{pred}\|_2 + w_f \|\mathbf{f} - \mathbf{f}^{pred}\|_2 + w_l \|\mathbf{r} \otimes (\mathbf{l} - \mathbf{l}^{pred})\|_2 \quad (11)$$

where \otimes expresses an element-wise product.

In this study, the number of batches for online learning is set to $N_{batch}^{online} = 10$, the number of epochs is set to $N_{epoch}^{online} = 10$, and other constants are set to $N_{thre}^{online} = 10$ and $N_{data}^{online} = 10$. N_{epoch}^{online} should be set much smaller than N_{epoch}^{init} , because if N_{epoch}^{online} is too large, RMAE will fit the obtained data too well and over-fitting will occur.

3.5. Controller Using RMAE

First, in this study, muscles of the musculoskeletal humanoid are controlled by the following muscle stiffness control [35],

$$\mathbf{f}^{send} = \mathbf{f}^{bias} + \max(\mathbf{0}, K_{stiff}(\mathbf{l}^{cur} - \mathbf{l}^{ref})) \quad (12)$$

where \mathbf{f}^{send} is a muscle tension to be exerted, \mathbf{f}^{bias} is a bias of muscle tension, and K_{stiff} is a muscle stiffness coefficient.

We describe a control method using RMAE. First, from the current muscle tension \mathbf{f}^{cur} and target joint angle θ^{ref} , the latent state is calculated as $\mathbf{z} = h_{enc,i}(\theta^{ref}, \mathbf{f}^{cur})$. Then, the following process is executed repeatedly.

- 1) Calculate $(\theta^{pred}, \mathbf{f}^{pred}, \mathbf{l}^{pred}) = h_{dec}(\mathbf{z})$.
- 2) Calculate the loss function $L_{control}(\theta^{pred}, \mathbf{f}^{pred}, \mathbf{l}^{pred})$.
- 3) Update \mathbf{z} using a backpropagation technique [33].

In 2), the loss function $L_{control}$ considering minimization of muscle tension and realization of target joint angle and necessary joint torque is calculated as below,

$$L_{control}(\theta, \mathbf{f}, \mathbf{l}) = w_1 \|\mathbf{f}\|_2 + w_2 \|\theta - \theta^{ref}\|_2 + w_3 \|\tau^{ref} + G^T(\theta^{ref}, \mathbf{f}^{cur})\mathbf{f}\|_2 \quad (13)$$

where $w_{\{1,2,3\}}$ is a constant weight, and τ^{ref} is a joint torque required to keep the posture of θ^{ref} , which is calculated from a geometric model. $G(\theta, \mathbf{f})$ is a muscle Jacobian, which is calculated from the difference of the outputs of \mathbf{l} when inputting $(\theta,$

\mathbf{f}) and $(\boldsymbol{\theta} + \Delta\boldsymbol{\theta}, \mathbf{f})$ to RMAE in the form of (i) ($\Delta\boldsymbol{\theta}$ is a small displacement of joint angle). In 3), \mathbf{z} is updated by a gradient descent with a backpropagation technique [33] as below,

$$\mathbf{g} = \partial L_{control} / \partial \mathbf{z} \quad (14)$$

$$\mathbf{z} = \mathbf{z} - \gamma \mathbf{g} / |\mathbf{g}| \quad (15)$$

where \mathbf{g} is a gradient of $L_{control}$ for \mathbf{z} , and γ is a learning rate. Although γ can be constant, batches are constructed with various γ in this study, and the best γ is selected at each step to achieve faster convergence. The maximum value of γ , $\gamma_{max}^{control}$, is determined, $[0, \gamma_{max}^{control}]$ is divided equally into $N_{batch}^{control}$ parts, and $N_{batch}^{control}$ batches of \mathbf{z} updated by each learning rate γ are created. 1) and 2) are executed again, and \mathbf{z} with the lowest $L_{control}$ is chosen. Steps 1)-3) are performed $N_{epoch}^{control}$ times. Finally, \mathbf{l}^{ref} considering muscle stiffness control of Eq. 12 is calculated as below using \mathbf{l}^{pred} and \mathbf{f}^{pred} obtained from \mathbf{z} , and is sent to the robot.

$$\mathbf{l}^{comp}(\mathbf{f}) = -(\mathbf{f} - \mathbf{f}^{bias}) / K_{stiff} \quad (16)$$

$$\mathbf{l}^{ref} = \mathbf{l}^{pred} + \mathbf{l}^{comp}(\mathbf{f}^{pred}) \quad (17)$$

This makes it possible to find \mathbf{l}^{ref} such that muscle tension is minimized in realizing the joint angle $\boldsymbol{\theta}^{ref}$. Although it is possible to directly calculate necessary muscle tension \mathbf{f}^{ref} by solving a quadratic programming minimizing $\|\mathbf{f}\|_2$ and satisfying $\boldsymbol{\tau}^{ref} = -G^T \mathbf{f}$, there is no guarantee that \mathbf{f}^{ref} can be realized at $\boldsymbol{\theta}^{ref}$. Therefore, in this study, \mathbf{f}^{ref} is searched for in the latent space \mathbf{z} .

Also, it is necessary to modify the control method for the muscle rupture information \mathbf{r} . Here, the muscle tension of the ruptured muscle i , f_i , must be zero. Therefore, Eq. 13 is partially modified to calculate the following loss,

$$L'_{control}(\boldsymbol{\theta}, \mathbf{f}, \mathbf{l}) = L_{control}(\boldsymbol{\theta}, \mathbf{f}, \mathbf{l}) + w_4 \|f_i\|_2 \quad (18)$$

where w_4 is a constant weight of which the value should be much larger than w_1 .

In this study, we set $w_1 = 1.0$, $w_2 = 1.0$, $w_3 = 0.01$, $w_4 = 10.0$, $\gamma_{max}^{control} = 0.5$, $N_{batch}^{control} = 10$, and $N_{epoch}^{control} = 10$.

3.6. State Estimator Using RMAE

Since joint angles cannot usually be measured in musculoskeletal humanoids as described in Sec. 2, the joint angle of the actual robot is estimated by using vision. However, in this case, it is necessary to attach markers to the robot and for the robot to keep looking at self-body at all times. By estimating the current joint angle through RMAE from the information on current muscle tension and length, it is possible to keep tracking the condition of the self-body. The state estimation method is simple: the current muscle tension \mathbf{f}^{cur} and the current muscle length \mathbf{l}^{cur} are obtained from the actual robot, these values are inputted to RMAE in the form of (ii) in Fig. 5, and then the estimated joint angle $\boldsymbol{\theta}^{est}$ is obtained as $\boldsymbol{\theta}^{est} = \mathbf{h}_{dec,\boldsymbol{\theta}}(\mathbf{h}_{enc,ii}(\mathbf{f}^{cur}, \mathbf{l}^{cur}))$.

Also, it is necessary for the state estimation method to be modified with the muscle rupture information \mathbf{r} . Since \mathbf{f} and \mathbf{l}

of the ruptured muscle i , f_i and l_i , cannot be trusted, the direct calculation of \mathbf{z} from $\mathbf{h}_{enc,ii}$ results in incorrect values. There are two possible ways to solve this problem.

The first method A is based on the assumption that there is no significant difference between the estimated joint angle in the previous frame $\boldsymbol{\theta}^{est,prev}$ and $\boldsymbol{\theta}^{cur}$. \mathbf{f}^{cur} of the ruptured muscle i , f_i^{cur} , is set to zero, $\mathbf{l}^{pred} = \mathbf{h}_{dec,l}(\boldsymbol{\theta}^{est,prev}, \mathbf{f}^{cur})$ is calculated, and \mathbf{l}^{cur} of the ruptured muscle i , l_i^{cur} , is updated as $l_i^{cur} = l_i^{pred}$. Then, as usual, $\boldsymbol{\theta}^{est}$ is calculated as $\boldsymbol{\theta}^{est} = \mathbf{h}_{dec,\boldsymbol{\theta}}(\mathbf{h}_{enc,ii}(\mathbf{f}^{cur}, \mathbf{l}^{cur}))$.

The second method A' is to update the latent variable \mathbf{z} in the same way as in Sec. 3.5. First, $\mathbf{z} = \mathbf{h}_{enc,ii}(\mathbf{f}^{cur}, \mathbf{l}^{cur})$ is calculated as with the unruptured muscle state. However, because f_i and l_i are unusual values, the same values of \mathbf{f} and \mathbf{l} cannot be reconstructed from $\mathbf{h}_{dec}(\mathbf{z})$. Therefore, the following loss function $L_{estimate}$ is calculated, and the current latent state \mathbf{z} is obtained by updating \mathbf{z} in the same way as in Sec. 3.5 (with the same parameters).

$$L_{estimate}(\mathbf{f}, \mathbf{l}) = w_5 \|f_i\|_2 + w_6 \|\mathbf{r} \otimes (\mathbf{f} - \mathbf{f}^{cur})\|_2 + w_7 \|\mathbf{r} \otimes (\mathbf{l} - \mathbf{l}^{cur})\|_2 \quad (19)$$

Finally, the estimated joint angle is obtained as $\boldsymbol{\theta}^{est} = \mathbf{h}_{dec,\boldsymbol{\theta}}(\mathbf{z})$.

Although it is clear that method A' is more accurate than method A, it is difficult to execute method A' with a fast cycle due to the high computational complexity of iterations. On the other hand, while method A is questionable in terms of the accuracy, it can be executed with a fast cycle.

In this study, we set $w_5 = 10.0$, $w_6 = 1.0$, and $w_7 = 1.0$.

3.7. Anomaly Detector Using RMAE

Data used in online learning is accumulated, and when the number of data exceeds N_{data}^{detect} , the model for anomaly detection is repeatedly rebuilt every time a new data is accumulated. At the same time, the data which exceeds N_{data}^{detect} are discarded in order from the oldest data. For all the obtained data $(\boldsymbol{\theta}, \mathbf{f}, \mathbf{l})$, the predicted values $\{\boldsymbol{\theta}, \mathbf{f}, \mathbf{l}\}^{pred}$ are calculated as $(\boldsymbol{\theta}^{pred}, \mathbf{f}^{pred}, \mathbf{l}^{pred}) = \mathbf{h}_{dec}(\mathbf{h}_{enc,ii}(\mathbf{f}, \mathbf{l}))$. For each muscle j , $\mathbf{v}_j = (f_j \quad l_j)^T$ and $\mathbf{v}_j^{pred} = (f_j^{pred} \quad l_j^{pred})^T$ are constructed. The average μ_e and covariance matrix Σ_e for all data of $\mathbf{e}_j = \mathbf{v}_j - \mathbf{v}_j^{pred}$ are calculated.

In the anomaly detection phase, \mathbf{f}^{cur} and \mathbf{l}^{cur} are always obtained, \mathbf{f}^{pred} and \mathbf{l}^{pred} are predicted, and the following value of Mahalanobis Distance is calculated for each muscle j .

$$\mathbf{e}_j = (\mathbf{f}_j^{cur} \quad \mathbf{l}_j^{cur})^T - (\mathbf{f}_j^{pred} \quad \mathbf{l}_j^{pred})^T \quad (20)$$

$$d_j = \sqrt{(\mathbf{e}_j - \mu_e)^T \Sigma_e^{-1} (\mathbf{e}_j - \mu_e)} \quad (21)$$

When d_j exceeds a threshold C_{thre}^{detect} , it is considered that an anomaly has emerged. When an anomaly is detected, the anomaly detection and online update of RMAE are stopped.

In this study, we set $N_{data}^{detect} = 50$, and $C_{thre}^{detect} = 30.0$. C_{thre}^{detect} is determined from preliminary experiments, since no anomalies are detected when the value is too low and anomalies continue to be detected when the value is too high.

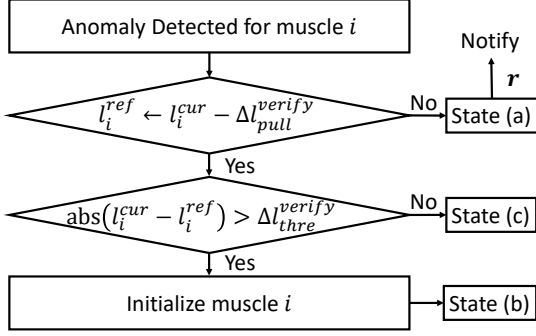


Figure 7: The procedure of muscle rupture verification.

3.8. Muscle Rupture Verification

When an anomaly is detected, it is necessary to verify the current state of the muscle rupture. In this study, we can consider the following states of muscles: (a) the muscle has broken or cannot transmit force due to failure of the motor, motor driver, etc., (b) the muscle has broken but can continue to be used depending on the broken part of the muscle wire, and (c) the muscle is not broken even though an anomaly is detected. The state (b) can occur when the end point of the muscle falls off of a fixed point or when the wire between the end point of the muscle and a nonlinear elastic element breaks. In this case, the nonlinear elastic element is trapped in a muscle relay unit that folds back the muscle, and although the origin of the muscle length is offset, it can still be used. The procedure for determining the muscle state is shown in Fig. 7.

The control of Eq. 12 ensures that the muscle is not loosened. In order to prevent overwinding of the muscle after the muscle rupture, l^{cur} is restricted to wind only Δl_{max}^{verify} from l^{ref} at maximum. The following procedure is performed for all muscles in which an anomaly is detected. First, if the muscle i is not ruptured and is working properly, the muscle tension will increase when l_i^{ref} is set to $l_i^{cur} - \Delta l_{pull}^{verify}$. In other words, if the change in muscle tension Δf_i exceeds Δf_{thre}^{verify} , it is considered that the muscle is working properly: state (b) or (c). If the muscle is not working properly, the muscle is assumed to be ruptured: state (a). Then, the muscle rupture information r with the value of muscle i as zero is notified to all components, and these execution methods are partially changed. If the muscle is working properly, we focus on the magnitude of $\text{abs}(l_i^{cur} - l_i^{ref})$. If this value is greater than Δl_{thre}^{verify} , the muscle state is considered to be (b), and if it is less than Δl_{thre}^{verify} , the muscle state is considered to be (c).

In the case of (b), although force is transmitted, the origin of the muscle length is offset and needs to be initialized. Here again, the same method as in Sec. 3.5 is used, where the latent variable z is repeatedly updated. First, the initial z is calculated as $z = h_{enc,i}(\theta^{cur}, f^{cur})$. Then, since values other than l_i^{cur} are correct, z representing the current state can be obtained by calculating the following loss function L_{verify} considering the match to the current joint angle, muscle tension, and muscle length, and by updating z in the same way as in Sec. 3.5 (with

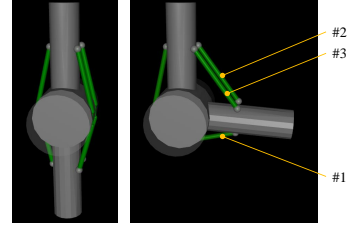


Figure 8: 1 DOF simple joint model in MuJoCo [36].

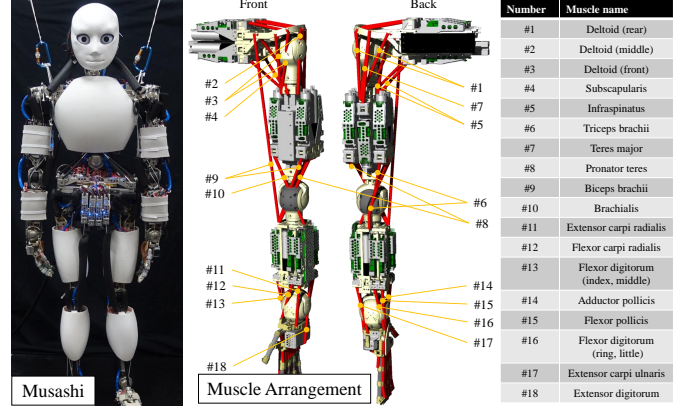


Figure 9: The musculoskeletal humanoid Musashi [1] and its muscle arrangement.

the same parameters),

$$L_{verify}(\theta, \mathbf{f}, \mathbf{l}) = w_8 \|\theta - \theta^{cur}\|_2 + w_9 \|\mathbf{f} - \mathbf{f}^{cur}\|_2 + w_{10} \|\mathbf{r}^{offset} \otimes (\mathbf{l} - \mathbf{l}^{cur})\|_2 \quad (22)$$

where \mathbf{r}^{offset} is an M -dimensional vector where only the offset muscle i is 0 and the rest are 1. Finally, the estimated muscle length is obtained from $\mathbf{l}^{est} = h_{dec,l}(z)$, and l_i^{cur} is initialized by l_i^{est} .

Since the body structure of the robot changes in the case of (a) and (b), the model of RMAE is stored in a different place and is restored after the muscle module is fixed or replaced. In addition, in the case of (a) and (b), all the accumulated data for constructing RMAE and the anomaly detection model are deleted. Once this procedure is finished for all the anomaly-detected muscles, the online learning of RMAE and updating of the anomaly detection model is resumed as usual.

In this study, we set $\Delta l_{max}^{verify} = 100$ [mm], $\Delta l_{pull}^{verify} = 10$ [mm], $\Delta f_{thre}^{verify} = 10$ [N], $\Delta l_{thre}^{verify} = 30$ [mm], $w_8 = 1.0$, $w_9 = 1.0$, and $w_{10} = 1.0$.

4. Experiments

4.1. Experimental Setup

First, a simple 1 DOF simulation is constructed using MuJoCo [36] (Fig. 8). The structure of the elbow is imitated, and 3 redundant muscles are arranged. Nonlinear elastic elements are arranged and friction loss is set in order to be closer to the actual robot. While the geometric model of the muscle route

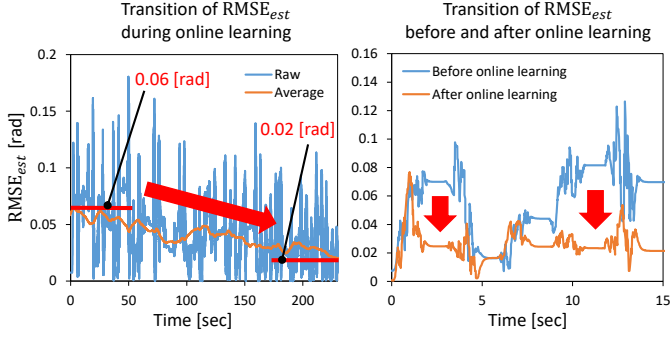


Figure 10: 1 DOF simulation experiment of state estimation without any muscle ruptured: transition of $RMSE_{est}$ during online learning (left graph), and comparison of $RMSE_{est}$ between before and after online learning (right graph).

is based on straight wire lines, the muscle route in simulation wraps around a cylinder of the elbow joint, and therefore requires learning of RMAE, just as in the actual robot.

Second, the musculoskeletal humanoid Musashi [1] is used (Fig. 9). There are 74 muscles in the body, and nonlinear elastic elements are placed at the ends of the muscles. Also, although ordinary musculoskeletal humanoids cannot measure joint angle, Musashi is equipped with a special mechanism called joint module, which can measure joint angle for experimental evaluation and can also be used as θ^{est} . Among the joints of Musashi, we mainly use 5 DOFs of the arm, denoted as S-p, S-r, S-y, E-p, and E-y (S and E expresses the shoulder and elbow, and rpy expresses roll, pitch and yaw, respectively). The number of muscles related to these 5 DOFs is 10, including 1 polyarticular muscle.

In this study, the effects of muscle rupture on each component and the behavior of changes in the components after muscle rupture are tested in both simulation and actual robot. The effectiveness of this study is demonstrated through a series of motion experiments with these components utilizing the redundant muscle arrangement. Note that for state estimation, the difference between the estimated joint angle θ^{est} obtained by Sec. 3.6 and the current joint angle of the robot θ^{cur} , $RMSE_{est} = \|\theta^{est} - \theta^{cur}\|_2$, is compared, and for control, the difference between the target joint angle θ^{ref} and θ^{cur} , $RMSE_{control} = \|\theta^{ref} - \theta^{cur}\|_2$, is compared. All the parameters set in this study are listed at the end of each subsection in Sec. 3.

4.2. 1 DOF Simulation Experiment

The online learning, state estimation, and control experiments are conducted using a simple 1 DOF joint simulator. In this section, θ is a 1-dimensional vector, and $\{l, f\}$ is a 3-dimensional vector.

4.2.1. Online Learning and State Estimator Experiment

First, we repeatedly send random joint angles θ^{rand} within the joint angle range, while executing the online learning of Sec. 3.4. Here, various states can be obtained as training data by not only using the control method of Sec. 3.5 but also sending the muscle length obtained from

$h_{dec,l}(h_{enc,i}(\theta^{rand}, f^{rand}))$ (f^{rand} is a random muscle tension). For each random joint angle, in turn, the muscle length is sent over 2 seconds by the method of Sec. 3.5, rests for 0.5 seconds, is sent over 1 second by the above method, and rests for another 0.5 seconds. This procedure is repeated. The left graph of Fig. 10 shows the transition of $RMSE_{est}$ and its average of every 20 seconds. The average of $RMSE_{est}$ decreased gradually from about 0.06 to 0.02 rad in 4 minutes. Then, five random joint angles θ^{rand} are specified, and in turn, muscle length is sent by the method of Sec. 3.5 over 2 seconds and rests for 0.5 seconds (we call this an evaluation experiment). The right graph of Fig. 10 shows how the transition of $RMSE_{est}$ changes when using RMAE before and after online learning. From this experiment onwards, online learning is not executed during the evaluation experiment. Most of the time, we found that $RMSE_{est}$ was smaller after the online learning than before. The results of the state estimator in 1 DOF simulation including the subsequent experiments are shown in Table 2. The average of $RMSE_{est}$ during 15 seconds of the evaluation experiment, $RMSE_{est}^{ave}$, was 0.056 rad before online learning and 0.026 rad after online learning.

Next, the left graph of Fig. 11 shows the transition of $RMSE_{est}$ when muscle #2 breaks and its muscle length is constant at 100 mm in the evaluation experiment. RMAE after the online learning as above is used. Here, we compare the three state estimations of Sec. 3.6, for without the muscle rupture information r and for two methods with r (A and A'). Method A' had the smallest error in 15 seconds, followed by method A and without r . $RMSE_{est}^{ave}$ was 0.40 rad without r , 0.13 rad for method A, and 0.037 rad for method A'. In all cases, the error was larger than 0.026 rad after the online learning of RMAE, and we can see that unlearned states were created due to the muscle rupture, which increased the error of state estimation.

Finally, the center and right graphs of Fig. 11 show the transitions of $RMSE_{est}$ after online learning with muscle #2 ruptured in the evaluation experiment. Here, we compare the online learnings in Sec. 3.4 for the cases without r (the center graph of Fig. 11) and with r (the right graph of Fig. 11). In each case, we compare the state estimations of Sec. 3.6 for without r and for the two methods with r (method A and A'). After the online learning without r , there was no significant difference of the transitions among three methods (without r , method A, and method A'), though the error of method A' was slightly smaller than that of others. $RMSE_{est}^{ave}$ was 0.17 rad for without r , 0.15 rad for method A, and 0.11 rad for method A'. Therefore, we found that the results after online learning without r were worse than before, regarding method A and A'. On the other hand, the joint angle errors after online learning with r were small in the order of method A', method A, and without r . $RMSE_{est}^{ave}$ was 0.73 rad without r , 0.097 rad for method A, and 0.021 rad for method A'. Therefore, we can see that the error of state estimation is reduced by continuing online learning with r , even if the muscle is ruptured. Note that in these experiments, method A can be executed at 100 Hz or higher, while method A' can only be executed at 10 Hz at most.

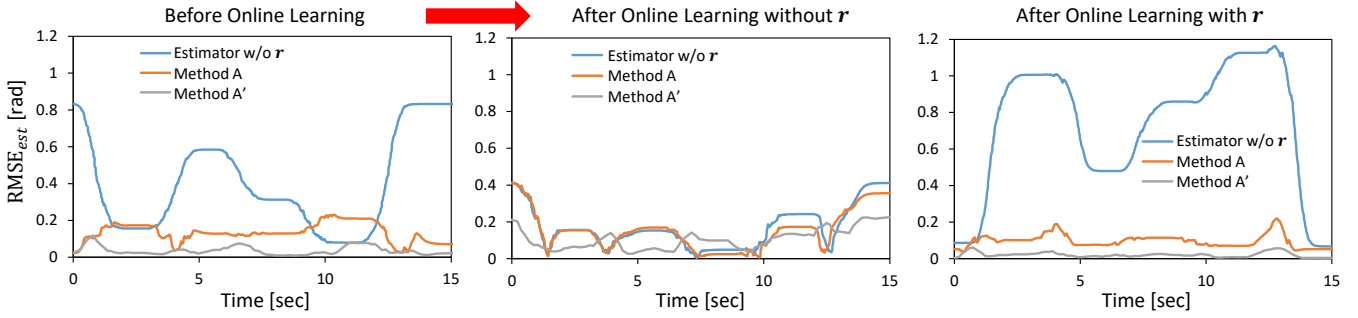


Figure 11: 1 DOF simulation experiment of state estimation when muscle #2 is ruptured: comparison of transitions of $RMSE_{est}$ among without r , with method A, and with method A', before online learning (left graph), after online learning without r (center graph), and after online learning with r (right graph).

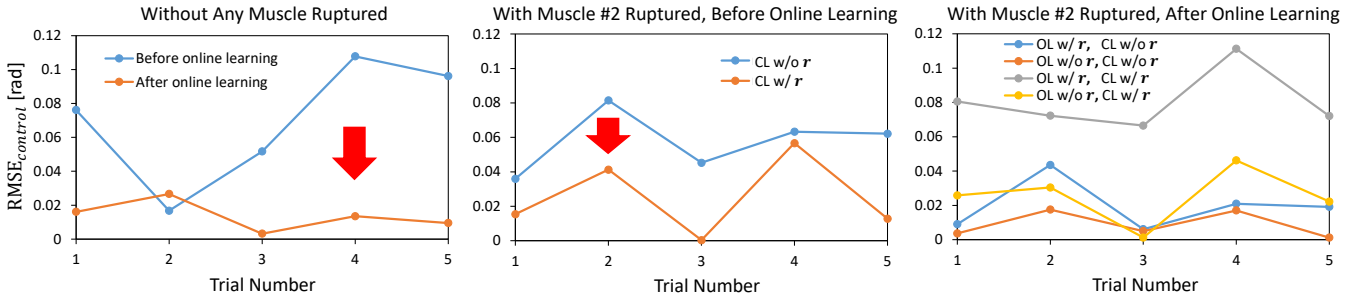


Figure 12: 1 DOF simulation experiment of controller: comparison of transitions of $RMSE_{control}$ between before and after online learning without any muscle ruptured (left graph), between using controller with or without r with muscle #2 ruptured (center graph), and between after online learning with or without r and using controller with or without r with muscle #2 ruptured (right graph). OL means online learning and CL means controller.

Table 2: Results of evaluation experiments for state estimator in 1 DOF simulation: the averages of $RMSE_{est}$ during 15 seconds of the evaluation experiment, $RMSE_{est}^{ave}$.

Muscle state	w/o rupture		w/ #2 ruptured		
	Before	After	Before	After, w/o r	After, w/ r
Estimator w/o r [rad]	0.056	0.026	0.40	0.17	0.73
Method A [rad]	-	-	0.13	0.15	0.097
Method A' [rad]	-	-	0.037	0.11	0.021

4.2.2. Online Learning and Controller Experiment

We execute the evaluation experiment as in Sec. 4.2.1 to see the control error. RMAEs before and after online learning in Sec. 4.2.1 are used for the controller, and $RMSE_{control}$ is calculated after each motion at rest. The results are shown in the left figure of Fig. 12. Although the magnitude of the error at the second joint angle was slightly reversed, we can see that the target joint angle was generally realized more accurately after online learning than before. The results of the controller in 1 DOF simulation including the subsequent experiments are shown in Table 3. The average of $RMSE_{control}^{ave}$ for the five joint angles, $RMSE_{control}^{ave}$, was 0.070 rad before online learning and 0.014 rad after online learning.

Next, we show the transition of $RMSE_{control}$ when muscle #2 is ruptured as in Sec. 4.2.1, in the center graph of Fig. 12. Here, we compare the controllers in Sec. 3.5 with and without r . We can see that the error of the controller with r was smaller than that without r regarding all joint angles. $RMSE_{control}^{ave}$ was 0.058 rad without r and 0.025 rad with r . Also, we can see that the error of joint angle after muscle rupture was larger than that before muscle rupture, regardless of with or without r .

Finally, we show the results of the evaluation experiment after online learning with the muscle ruptured, in the right figure of Fig. 12. Here, we compare the online learnings of Sec. 3.4 with and without r . For each case, we also compare the controllers of Sec. 3.5 with and without r . The results show that the error was smaller when r was available for the controller, in each case after online learning with or without r . Similarly, for the online learning, we can see that the error was smaller when r was available.

Table 3: Results of evaluation experiments for controller in 1 DOF simulation: the averages of $RMSE_{control}$ for the five joint angles of the evaluation experiment, $RMSE_{control}^{ave}$.

Muscle state	w/o rupture		w/ #2 ruptured		
	Before	After	Before	After, w/o r	After, w/ r
Online learning	0.070	0.014	0.058	0.081	0.020
Controller w/o r [rad]	-	-	0.025	0.025	0.0089
Controller w/ r [rad]	-	-	-	-	-

4.3. Actual Robot Experiment

The online learning, state estimation, control, anomaly detection, and muscle rupture verification experiments are conducted using the actual robot of the left arm of Musashi. In this section, θ is a 5-dimensional vector, and $\{l, f\}$ is a 10 dimensional vector.

4.3.1. Online Learning and State Estimator Experiment

We show the transitions of state estimation errors $RMSE_{est}$ before and after online learning of RMAE with the actual robot of Musashi (Fig. 13) during the evaluation experiment as in

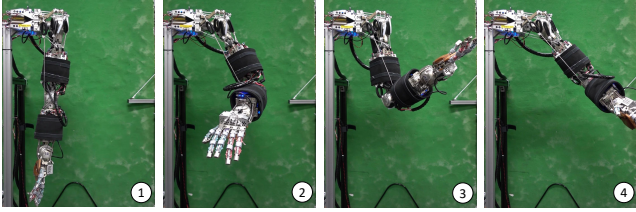


Figure 13: Actual robot experiment of online learning: these pictures show the random movements after online learning of RMAE without any muscle ruptured.

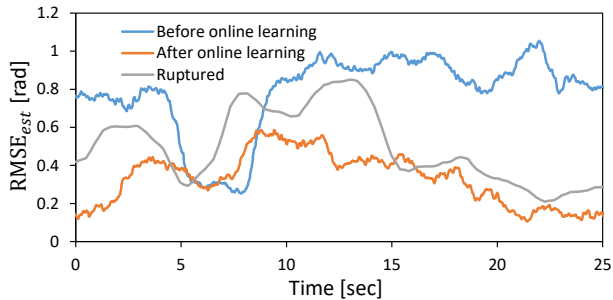


Figure 14: Actual robot experiment of state estimation: comparison of transitions of $RMSE_{est}$ among before online learning, after online learning, and when muscle #9 is ruptured.

Sec. 4.2.1, in Fig. 14. Fig. 14 also shows the transition when muscle #9 is ruptured (the current of the motor is set to zero) and when using method A' with RMAE after the online learning for the state estimation. The following evaluation experiment is basically the same as in Sec. 4.2.1, but the number of random joint angles to be sent is increased to 7 and they are sent over 3 seconds. From the results, we can see that the error of the state estimation was much smaller after the online learning than before. When the muscle was ruptured, the error became slightly larger than after the online learning. The results of the state estimator in the actual robot including the subsequent experiments are shown in Table 4. The average of $RMSE_{est}^{ave}$ during 25 seconds of this motion, $RMSE_{est}^{ave}$, was 0.78 rad before online learning, 0.33 rad after online learning, and 0.50 rad after the muscle rupture.

Next, Fig. 15 shows the transition of $RMSE_{est}$ after online learning with the muscle ruptured. Here, we compare the transitions of the error when using method A' in Sec. 3.6 (the method with the best performance in Sec. 4.2.1) after the online learning in Sec. 3.4 with and without r . We can see that the error was smaller with r than without r . Without r , the error was sometimes smaller or larger than before the online learning, and the error did not vary so much. $RMSE_{est}^{ave}$ was 0.44 rad without r , and 0.27 rad with r . Therefore, the online learning with r can maintain the same or lower error after the muscle rupture than that before the muscle rupture.

4.3.2. Online Learning and Controller Experiment

We execute the evaluation experiment as in Sec. 4.3.1 to see the control error. Here, RMAEs before and after online learning in Sec. 4.3.1 are used for the controller, and $RMSE_{control}$ is calculated after each motion at rest. In this section, we perform the same motion five times, and display the average and variance of

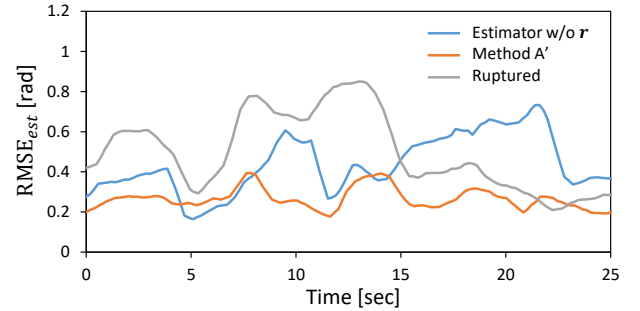


Figure 15: Actual robot experiment of state estimation with muscle #9 ruptured: comparison of transitions of $RMSE_{est}$ between after online learning with and without r .

Table 4: Results of evaluation experiments for state estimator in the actual robot: the averages of $RMSE_{est}$ during 25 seconds of the evaluation experiment, $RMSE_{est}^{ave}$.

Muscle state	w/o rupture		w/ #9 ruptured		
	Before	After	Before	After, w/o r	After, w/ r
Online learning	0.78	0.33	-	-	-
Estimator w/o r [rad]	-	-	0.50	0.44	0.27
Method A' [rad]	-	-	-	-	-

the errors. The results are shown in Fig. 16. Regarding RMAE after the online learning, we also show the results of the controller in Sec. 3.5 with r , where muscle #9 is ruptured. Except for the fourth joint angle, we can see that the error was smaller after the online learning than before. In addition, the error did not change significantly when the muscle is ruptured, unlike the state estimation. This seems to be due to the fact that the online learning was successful for the robot state without muscle #9. Also, the variance of the error was very small. The results of the controller in the actual robot including the subsequent experiments are shown in Table 5. The average of $RMSE_{control}$ for the seven joint angles, $RMSE_{control}^{ave}$, was 0.64 rad before online learning, 0.36 rad after online learning, and 0.37 rad after the muscle rupture.

Next, Fig. 17 shows the average of $RMSE_{control}$ after the online learning with the muscle ruptured. Here, we compare the online learnings in Sec. 3.4 with and without r . Note that the muscle length is controlled by including r in Sec. 3.5. Although the results differed depending on the posture, we see that the error was smaller with r than without, and that the results were equivalent to those of the simulation. $RMSE_{control}^{ave}$ was 0.35 rad without r and 0.25 rad with r .

Table 5: Results of evaluation experiments for controller in the actual robot: the averages of $RMSE_{control}$ for the seven joint angles of the evaluation experiment.

Muscle state	w/o rupture		w/ #2 ruptured		
	Before	After	Before	After, w/o r	After, w/ r
Online learning	0.64	0.36	-	-	-
Controller w/o r [rad]	-	-	0.37	0.35	0.25
Controller w/ r [rad]	-	-	-	-	-

4.3.3. Anomaly Detection and Muscle Rupture Verification Experiment

In this experiment, a muscle wire is actually cut and we test for anomaly detection and muscle rupture verification methods.

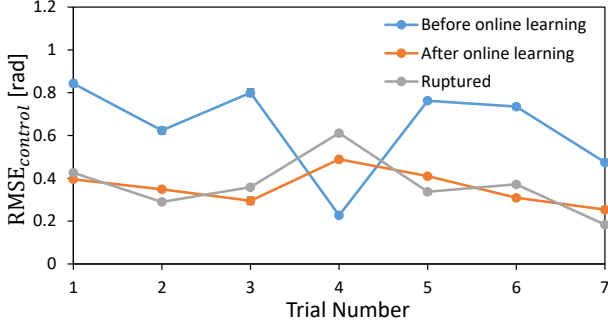


Figure 16: Actual robot experiment of controller: comparison of transitions of $RMSE_{control}$ among before online learning, after online learning, and when muscle #9 is ruptured.

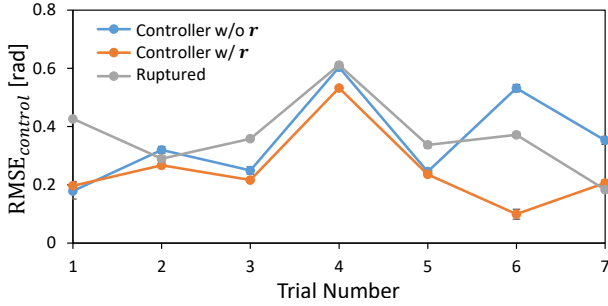


Figure 17: Actual robot experiment of controller with muscle #9 ruptured: comparison of transitions of $RMSE_{control}$ between after online learning with and without r .

First, we investigate how the anomaly detection and muscle rupture verification work when muscle #9 is cut with scissors. The degree of anomaly d_j and muscle length of muscle #9, and muscle tensions of muscles #8 and #9 are shown in Fig. 18 for the following series of motions: a random motion sending random joint angles, cutting the muscle, and then the random motion again, in order. Note that muscles #8 and #9 are synergistic muscles with similar moment arms. During the random motion, the muscle tension of #8 and #9 was about 69 N and 38 N at most. When muscle #9 was cut, the muscle tension became zero, the muscle length was gradually shortened due to f_{bias} , and d_j exceeded $C_{thre}^{detect} = 30.0$ (d_j of other muscles did not change much). The difference between the target and measured muscle lengths stopped at $\Delta l_{max}^{verify} = 100$ [mm], which was set as the maximum value. After that, the target muscle length changed to $l_i^{cur} - \Delta l_{pull}^{verify}$ ($\Delta l_{pull}^{verify} = 10$ [mm]), but the muscle tension did not change at all because the muscle was broken. Therefore, #9 was judged to be ruptured (state (a)) and r was notified to all components. After that, the robot could move its joints as usual, but no tension was applied to muscle #9 and about 100 N was applied to muscle #8.

We next investigate how the anomaly detection and muscle rupture verification work when the end point of muscle #8 has been taken off. The degree of anomaly d_j and muscle length of muscle #8, and muscle tensions of muscles #8 and #9 are shown in Fig. 19 for a series of motions of bending the elbow, cutting the muscle, and then performing a random motion, in order. After the muscle rupture of #8, the muscle length was gradually shortened by f_{bias} , and d_j of muscle #8 exceeded

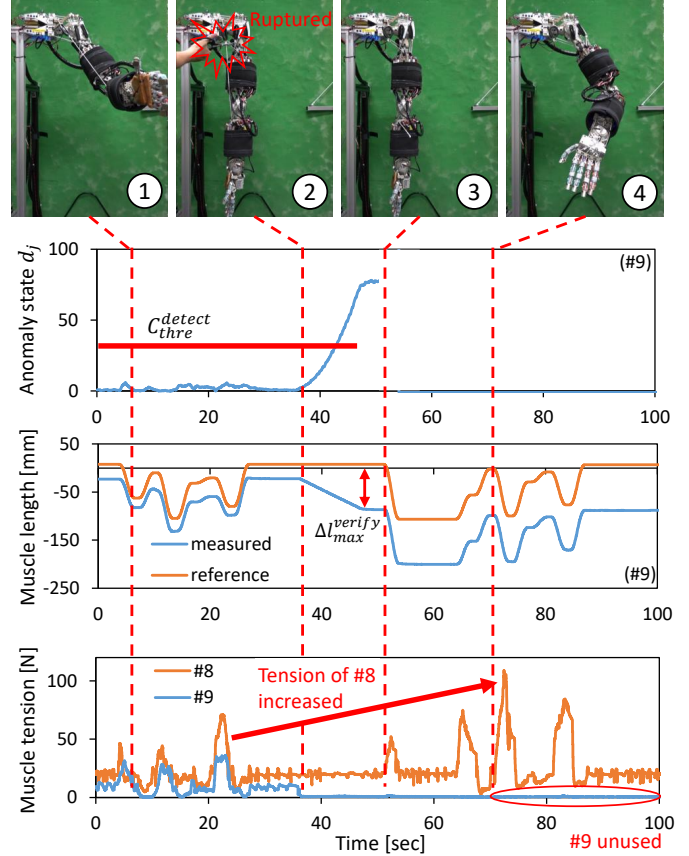


Figure 18: Actual robot experiment of anomaly detection and muscle rupture verification when the muscle wire of muscle #9 is ruptured: the transitions of anomaly state d_j and muscle length of muscle #9, and transition of muscle tension of muscle #8 and #9.

$C_{thre}^{detect} = 30.0$ (d_j of other muscles did not change much). The difference between the target and measured muscle lengths stopped at 57 mm, which was smaller than the maximum value $\Delta l_{max}^{verify} = 100$ [mm]. Thereafter, the target muscle length was changed to $l_i^{cur} - \Delta l_{pull}^{verify}$ ($\Delta l_{pull}^{verify} = 10$ [mm]), and l_i^{cur} followed it, resulting in an increase in muscle tension of about 180 N. Since $\Delta f_i > \Delta f_{thre}^{verify}$ ($\Delta f_{thre}^{verify} = 10$ [N]) and $abs(l_i^{cur} - l_i^{ref}) > \Delta l_{thre}^{verify}$ ($\Delta l_{thre}^{verify} = 30$ [mm]), muscle #8 was determined to be in state (b) and the muscle length was initialized. After that, the robot could move its joints as usual, and a muscle tension of about 120 N was applied to muscle #8.

4.4. Continuous Motion Experiment by Musashi

The musculoskeletal humanoid Musashi is used to perform a box manipulation experiment, and a series of events including muscle rupture, anomaly detection, muscle rupture verification, and online learning occur. The robot holds a large box with both hands and puts it down. During this experiment, online learning is executed at all times.

Muscle #9 of the left arm is cut with scissors before holding the box. Here, we compare the cases of whether the muscle rupture verification in Sec. 4.3.3 is executed or not. With the muscle rupture verification, r is notified to all the components, while without it, r is not taken into account for online learning,

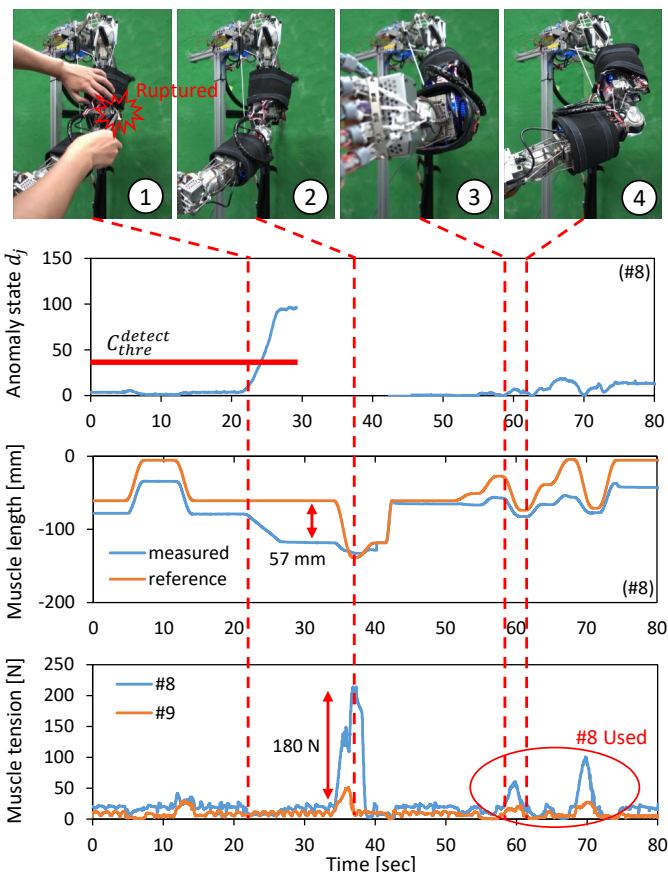


Figure 19: Actual robot experiment of anomaly detection and muscle rupture verification when the endpoint of muscle #8 is ruptured: the transitions of anomaly state d_j and muscle length of muscle #8, and transition of muscle tension of muscle #8 and #9.

controller, and state estimation even if the muscle is ruptured. Then, as in Sec. 4.3.2, the left arm is moved by random joint angles and muscle tensions for online learning of RMAE. We then resume the box manipulation experiment (online learning continues to work during this time). Here, we set $N_{thre}^{online} = 2$ so that the online learning starts immediately.

Fig. 20 shows the case without the muscle rupture verification and Fig. 21 shows the case with the muscle rupture verification. When the muscle rupture verification was not performed, online learning proceeded with muscle length of one muscle with a strange value, so the robot could not raise its left hand as expected and dropped the box. In contrast, in the case with the muscle rupture verification, both hands worked well together and the box was manipulated correctly after resumption of the manipulation, because the muscle rupture information r was notified and the online learning progressed correctly.

5. Discussion

Based on the experimental results of this study, we discuss the effects of muscle rupture on online learning, state estimation, and control using RMAE.

First, it is possible to see the ideal performance of RMAE in the simple 1 DOF simulation experiments. In the online learn-

ing method, RMAE can reduce the error of the joint angle estimation by one third in 4 minutes. In the state estimation, the error can be greatly reduced by using the muscle rupture information r when the muscle breaks. Although the computational cost of method A' is more expensive, it can achieve higher accuracy than method A. It is also found that while the estimation error is extremely large when updating RMAE online without r after a muscle rupture, the estimation error can be reduced even further by changing the online learning method using r . This tendency is also true for the controller using RMAE, where online learning of RMAE significantly reduces the control error. By using the information of r , the control error can be further reduced by online learning after the muscle rupture.

Next, in the experiment on the 5 DOFs of the left shoulder and elbow of Musashi, we found out by how much the performance of components using RMAE is affected by the characteristics of the actual robot. For the state estimation, we can see that the tendency of the estimation error is almost the same as that of the simulation, and that the online learning of RMAE improves the error significantly. However, although the peak of the error can be suppressed, we cannot see as large a difference between methods A and A' as in the simulation. This is considered to be because RMAE is not updated as completely as in the simulation, and therefore the difference between methods A and A' is lost in the error of RMAE. In addition, the control error can be reduced by online learning, and online learning with r is effective as well. However, in general, the difference between with and without r is smaller than that of the simulation, and the error depends greatly on the posture of the robot. It is also found that the anomaly detection and muscle rupture verification are able to correctly determine the current state of the muscles, to recognize muscles that are not usable and notify r to all components, and to initialize and reuse muscles that are usable but are offset in the initial muscle length.

Finally, in the box manipulation experiment describing the overall flow of this study, it is found that there is a significant difference in task execution depending on the presence or absence of the muscle rupture information r . If the online learning process is continued without r , the abnormal sensor values of the ruptured muscle deteriorate the entire network, and the target task fails.

From this study, we found that in order to take advantage of the redundant muscle arrangement, it is necessary to recognize the muscle rupture and process it appropriately to perform online learning, state estimation, and control of the flexible body structure. It is also important to construct a whole system that includes replaceable hardware, anomaly detection, and muscle rupture verification. We believe that our method may be one of the methods that can cope with malfunctions of the robot, such as the failure of some sensors and drive systems. In addition, because there are some muscles that cannot be compensated if they are ruptured, our research limits the muscles that can be ruptured (#2, #8, and #9). In future works, we would like to develop a design optimization method of the muscle arrangement so that any muscle rupture can be compensated.

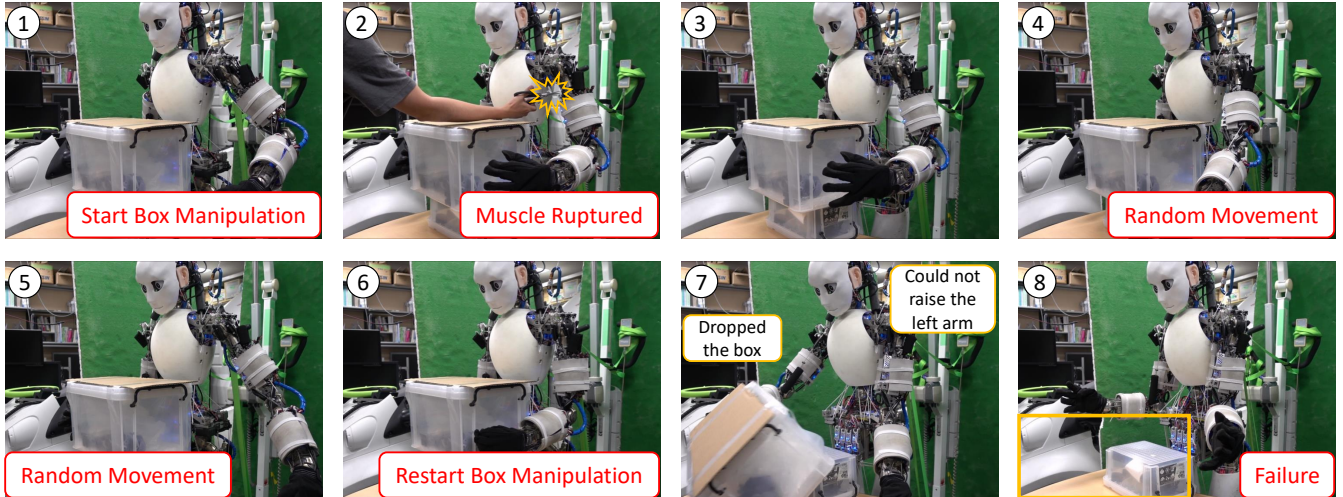


Figure 20: Continuous motion experiment by Musashi without muscle rupture verification: Musashi starts box manipulation, muscle rupture occurs, RMAE is updated online during random movements, Musashi restarts box manipulation, but Musashi dropped the box because its left arm could not be raised as expected.

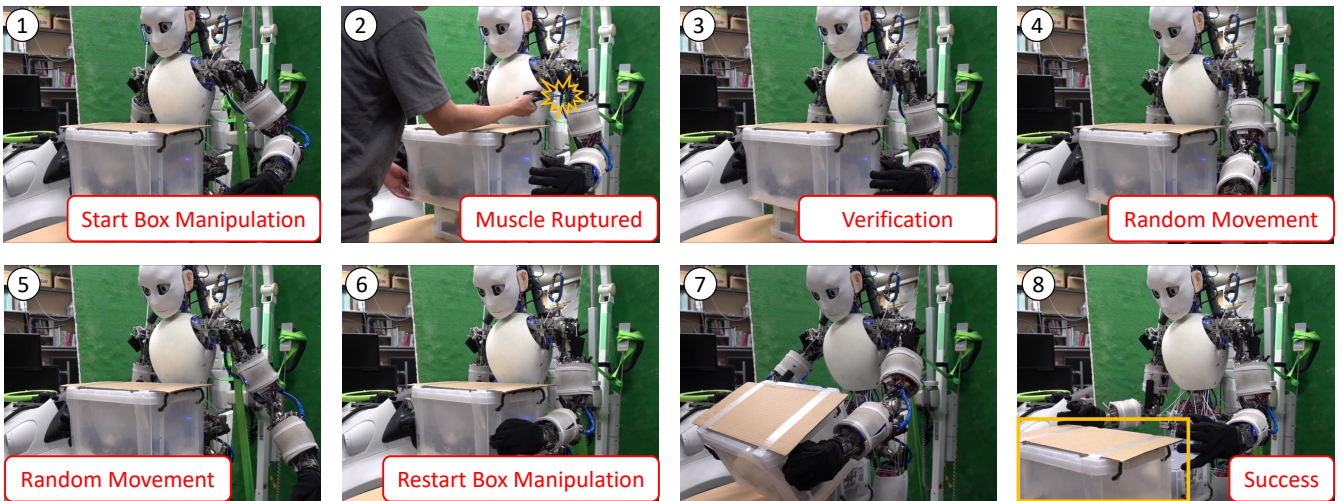


Figure 21: Continuous motion experiment by Musashi with muscle rupture verification: Musashi starts box manipulation, muscle rupture occurs, muscle rupture verification is executed to notify muscle rupture state r to all components, RMAE is updated online during random movements, Musashi restarts box manipulation, and Musashi succeeded in putting the box down with both arms.

6. Conclusion

In this study, we proposed a new learning control method making use of the characteristic that the redundant musculoskeletal humanoid can keep moving its joints even when one of its redundant muscles is ruptured. The redundant musculoskeletal autoencoder (RMAE), which expresses redundant intersensory relationships among joint angle, muscle tension, and muscle length, is constructed and used for the state estimation and control of the flexible and difficult-to-modelize body by updating RMAE online. Anomaly is detected from the prediction error of RMAE, and muscle rupture is verified by moving the muscles one by one. When a muscle rupture occurs, the online learning, state estimation, and control algorithms are modified based on the muscle rupture information to adapt to the current robot condition without destroying the current network structure of RMAE. Experimental results show that the presence or absence of the muscle rupture information significantly affects

the errors in control and state estimation, and the effectiveness of this study was confirmed through a box manipulation experiment.

In future works, we will continue to run these systems for a long time in order to construct a more robust robot system.

References

- [1] K. Kawaharazuka, S. Makino, K. Tsuzuki, M. Onitsuka, Y. Nagamatsu, K. Shinjo, T. Makabe, Y. Asano, K. Okada, K. Kawasaki, M. Inaba, Component Modularized Design of Musculoskeletal Humanoid Platform Musashi to Investigate Learning Control Systems, in: Proceedings of the 2019 IEEE/RSJ International Conference on Intelligent Robots and Systems, 2019, pp. 7294–7301.
- [2] Y. Nakanishi, S. Ohta, T. Shirai, Y. Asano, T. Kozuki, Y. Kakehashi, H. Mizoguchi, T. Kurotobi, Y. Motegi, K. Sasabuchi, J. Urata, K. Okada, I. Mizuuchi, M. Inaba, Design Approach of Biologically-Inspired Musculoskeletal Humanoids, International Journal of Advanced Robotic Systems 10 (4) (2013) 216–228.

- [3] S. Wittmeier, C. Alessandro, N. Bascarevic, K. Dalamagkidis, D. Devereux, A. Diamond, M. Jäntschi, K. Jovanovic, R. Knight, H. G. Marques, P. Milosavljevic, B. Mitra, B. Svetozarevic, V. Potkonjak, R. Pfeifer, A. Knoll, O. Holland, *Toward Anthropomorphic Robotics: Development, Simulation, and Control of a Musculoskeletal Torso*, *Artificial Life* 19 (1) (2013) 171–193.
- [4] M. Jäntschi, S. Wittmeier, K. Dalamagkidis, A. Panos, F. Volkart, A. Knoll, *Anthrob - A Printed Anthropomorphic Robot*, in: *Proceedings of the 2013 IEEE-RAS International Conference on Humanoid Robots*, 2013, pp. 342–347.
- [5] Y. Asano, T. Kozuki, S. Ookubo, M. Kawamura, S. Nakashima, T. Katayama, Y. Iori, H. Toshinori, K. Kawaharazuka, S. Makino, Y. Kakiuchi, K. Okada, M. Inaba, *Human Mimetic Musculoskeletal Humanoid Kengoro toward Real World Physically Interactive Actions*, in: *Proceedings of the 2016 IEEE-RAS International Conference on Humanoid Robots*, 2016, pp. 876–883.
- [6] K. Kawaharazuka, K. Tsuzuki, S. Makino, M. Onitsuka, Y. Asano, K. Okada, K. Kawasaki, M. Inaba, *Long-time Self-body Image Acquisition and its Application to the Control of Musculoskeletal Structures*, *IEEE Robotics and Automation Letters* 4 (3) (2019) 2965–2972.
- [7] M. A. Sharbafi, C. Rode, S. Kurowski, D. Scholz, R. Möckel, K. Radkhah, G. Zhao, A. M. Rashty, O. V. Stryk, A. Seyfarth, *A new biarticular actuator design facilitates control of leg function in BioBiped3*, *Bioinspiration & Biomimetics* 11 (4) (2016) 046003.
- [8] S. Zhong, J. Chen, X. Niu, H. Fu, H. Qiao, *Reducing Redundancy of Musculoskeletal Robot with Convex Hull Vertexes Selection*, *IEEE Transactions on Cognitive and Developmental Systems* (2019) 1–1.
- [9] C. Alessandro, I. Delis, F. Nori, S. Panzeri, B. Berret, *Muscle synergies in neuroscience and robotics: from input-space to task-space perspectives*, *Frontiers in Computational Neuroscience* 7 (43) (2013) 1–16.
- [10] M. Kawamura, S. Ookubo, Y. Asano, T. Kozuki, K. Okada, M. Inaba, *A Joint-Space Controller Based on Redundant Muscle Tension for Multiple DOF Joints in Musculoskeletal Humanoids*, in: *Proceedings of the 2016 IEEE-RAS International Conference on Humanoid Robots*, 2016, pp. 814–819.
- [11] M. Jäntschi, C. Schmalzer, S. Wittmeier, K. Dalamagkidis, A. Knoll, *A scalable joint-space controller for musculoskeletal robots with spherical joints*, in: *Proceedings of the 2011 IEEE International Conference on Robotics and Biomimetics*, 2011, pp. 2211–2216.
- [12] M. Jäntschi, S. Wittmeier, K. Dalamagkidis, A. Knoll, *Computed muscle control for an anthropomorphic elbow joint*, in: *Proceedings of the 2012 IEEE/RSJ International Conference on Intelligent Robots and Systems*, 2012, pp. 2192–2197.
- [13] S. Ookubo, Y. Asano, T. Kozuki, T. Shirai, K. Okada, M. Inaba, *Learning Nonlinear Muscle-Joint State Mapping Toward Geometric Model-Free Tendon Driven Musculoskeletal Robots*, in: *Proceedings of the 2015 IEEE-RAS International Conference on Humanoid Robots*, 2015, pp. 765–770.
- [14] Y. Motegi, T. Shirai, T. Izawa, T. Kurotobi, J. Urata, Y. Nakanishi, K. Okada, M. Inaba, *Motion control based on modification of the Jacobian map between the muscle space and work space with musculoskeletal humanoid*, in: *Proceedings of the 2012 IEEE-RAS International Conference on Humanoid Robots*, 2012, pp. 835–840.
- [15] I. Mizuuchi, Y. Nakanishi, T. Yoshikai, M. Inaba, H. Inoue, O. Khatib, *Body Information Acquisition System of Redundant Musculo-Skeletal Humanoid*, in: *Experimental Robotics IX*, 2006, pp. 249–258.
- [16] K. Kawaharazuka, S. Makino, M. Kawamura, Y. Asano, K. Okada, M. Inaba, *Online Learning of Joint-Muscle Mapping using Vision in Tendon-driven Musculoskeletal Humanoids*, *IEEE Robotics and Automation Letters* 3 (2) (2018) 772–779.
- [17] K. Kawaharazuka, S. Makino, M. Kawamura, A. Fujii, Y. Asano, K. Okada, M. Inaba, *Online Self-body Image Acquisition Considering Changes in Muscle Routes Caused by Softness of Body Tissue for Tendon-driven Musculoskeletal Humanoids*, in: *Proceedings of the 2018 IEEE/RSJ International Conference on Intelligent Robots and Systems*, 2018, pp. 1711–1717.
- [18] D. Büchler, R. Calandra, B. Schölkopf, J. Peters, *Control of Musculoskeletal Systems Using Learned Dynamics Models*, *IEEE Robotics and Automation Letters* 3 (4) (2018) 3161–3168.
- [19] D. Driess, H. Zimmermann, S. Wolfen, D. Suissa, D. Haeuffle, D. Hennes, M. Toussaint, S. Schmitt, *Learning to Control Redundant Musculoskeletal Systems with Neural Networks and SQP: Exploiting Muscle Properties*, in: *Proceedings of the 2018 IEEE International Conference on Robotics and Automation*, 2018, pp. 6461–6468.
- [20] Z. Xie, L. Jin, X. Luo, S. Li, X. Xiao, *A Data-Driven Cyclic-Motion Generation Scheme for Kinematic Control of Redundant Manipulators*, *IEEE Transactions on Control Systems Technology* 29 (1) (2021) 53–63.
- [21] Y. Huang, D. Büchler, O. Koç, B. Schölkopf, J. Peters, *Jointly learning trajectory generation and hitting point prediction in robot table tennis*, in: *Proceedings of the 2016 IEEE-RAS International Conference on Humanoid Robots*, 2016, pp. 650–655.
- [22] K. Kawaharazuka, K. Tsuzuki, M. Onitsuka, Y. Asano, K. Okada, K. Kawasaki, M. Inaba, *Musculoskeletal AutoEncoder: A Unified Online Acquisition Method of Intersensory Networks for State Estimation, Control, and Simulation of Musculoskeletal Humanoids*, *IEEE Robotics and Automation Letters* 5 (2) (2020) 2411–2418.
- [23] A. D. Luca, A. Albu-Schaffer, S. Haddadin, G. Hirzinger, *Collision Detection and Safe Reaction with the DLR-III Lightweight Manipulator Arm*, in: *Proceedings of the 2006 IEEE/RSJ International Conference on Intelligent Robots and Systems*, 2006, pp. 1623–1630.
- [24] D. Park, Y. Hoshi, C. C. Kemp, *A Multimodal Anomaly Detector for Robot-Assisted Feeding Using an LSTM-Based Variational Autoencoder*, *IEEE Robotics and Automation Letters* 3 (3) (2018) 1544–1551.
- [25] E. Principi, D. Rossetti, S. Squartini, F. Piazza, *Unsupervised electric motor fault detection by using deep autoencoders*, *IEEE/CAA Journal of Automatica Sinica* 6 (2) (2019) 441–451.
- [26] J. Urata, Y. Nakanishi, A. Miyadera, I. Mizuuchi, T. Yoshikai, M. Inaba, *A Three-Dimensional Angle Sensor for a Spherical Joint Using a Micro Camera*, in: *Proceedings of the 2006 IEEE International Conference on Robotics and Automation*, 2006, pp. 4428–4430.
- [27] S. Nakashima, T. Shirai, K. Kawaharazuka, Y. A. Y. Kakiuchi, K. Okada, M. Inaba, *An Approach of Facilitated Investigation of Active Self-healing Tension Transmission System Oriented for Legged Robots*, in: *Proceedings of the 2019 IEEE/RSJ International Conference on Intelligent Robots and Systems*, 2019, pp. 2567–2572.
- [28] Y. Asano, T. Kozuki, S. Ookubo, K. Kawasaki, T. Shirai, K. Kimura, K. Okada, M. Inaba, *A Sensor-driver Integrated Muscle Module with High-tension Measurability and Flexibility for Tendon-driven Robots*, in: *Proceedings of the 2015 IEEE/RSJ International Conference on Intelligent Robots and Systems*, 2015, pp. 5960–5965.
- [29] K. Kawaharazuka, S. Makino, M. Kawamura, Y. Asano, Y. Kakiuchi, K. Okada, M. Inaba, *Human Mimetic Forearm Design with Radioulnar Joint using Miniature Bone-muscle Modules and its Applications*, in: *Proceedings of the 2017 IEEE/RSJ International Conference on Intelligent Robots and Systems*, 2017, pp. 4956–4962.
- [30] T. Kozuki, Y. Motegi, T. Shirai, Y. Asano, J. Urata, Y. Nakanishi, K. Okada, M. Inaba, *Design of upper limb by adhesion of muscles and bones - Detail human mimetic musculoskeletal humanoid kenshiro*, in: *Proceedings of the 2013 IEEE/RSJ International Conference on Intelligent Robots and Systems*, 2013, pp. 935–940.
- [31] G. E. Hinton, R. R. Salakhutdinov, *Reducing the Dimensionality of Data with Neural Networks*, *Science* 313 (5786) (2006) 504–507.
- [32] S. Tokui, K. Oono, S. Hido, J. Clayton, *Chainer: a next-generation open source framework for deep learning*, in: *Proceedings of Workshop on Machine Learning Systems in The 29th Annual Conference on Neural Information Processing Systems*, 2015.
- [33] D. E. Rumelhart, G. E. Hinton, R. J. Williams, *Learning representations by back-propagating errors*, *nature* 323 (6088) (1986) 533–536.
- [34] D. P. Kingma, J. Ba, *Adam: A Method for Stochastic Optimization*, in: *Proceedings of the 3rd International Conference on Learning Representations*, 2015, pp. 1–15.
- [35] T. Shirai, J. Urata, Y. Nakanishi, K. Okada, M. Inaba, *Whole body adapting behavior with muscle level stiffness control of tendon-driven multi-joint robot*, in: *Proceedings of the 2011 IEEE International Conference on Robotics and Biomimetics*, 2011, pp. 2229–2234.
- [36] E. Todorov, T. Erez, Y. Tassa, *MuJoCo: A physics engine for model-based control*, in: *Proceedings of the 2012 IEEE/RSJ International Conference on Intelligent Robots and Systems*, 2012, pp. 5026–5033.